Published in final edited form as:
Heart Rhythm. 2008 June ; 5(6): 846–854. doi:10.1016/j.hrthm.2008.03.010.

Rotor Meandering Contributes to Irregularity in Electrograms during Atrial Fibrillation

Sharon Zlochiver, PhD, **Masatoshi Yamazaki, MD**, **Jerome Kalifa, MD, PhD**, and **Omer Berenfeld, PhD**
Center for Arrhythmia Research, University of Michigan, Ann Arbor, MI

Abstract

Radiofrequency ablation therapy of atrial fibrillation (AF) recently incorporated the analysis of dominant frequency (DF) and/or electrogram fractionation for guidance. However, the relationships between DF, fractionation and spatio-temporal characteristics of the AF source remain unclear. We hypothesize that meandering reentrant AF source contributes to the wave fractionation and is reflected in the power spectrum of local electrograms elsewhere in the rotor's surroundings.

Methods—Meandering rotors as AF sources were simulated in 2D models of human atrial tissue and recorded in isolated sheep hearts. Non-dominant elements of the signals were differentiated from the dominant elements using singular value decomposition, whereby the purely periodic constituent (PC) relating to the rotor's DF was eliminated rendering a residual constituent (RC) that consisted of all other activity.

Results—Spectral analysis of the decomposed constituents revealed peaks corresponding to the meandering frequency of the rotor tip, the magnitudes of which were proportional to the size of, and the distance to the rotor core. Similar analyses on epicardial optical signals and electrograms from isolated sheep hearts, as well as human complex fractionated atrial electrograms demonstrated applicability of the approach.

Conclusion—Increased meandering of the rotor driving AF reduces activation periodicity and increases fractionation. The spectral manifestation of the rotor activity beyond the meandering region makes it possible to characterize AF source stability, as well as DF in humans using electrode mapping.

Keywords

Electrocardiography; mapping; arrhythmia; Fourier analysis

Introduction

The mechanisms underlying atrial fibrillation (AF) are poorly understood[1] resulting in limited success of ablative and pharmacological procedures. The characterization of the spatio-temporal organization of the myocardial electrical activity during fibrillation in experimental models has been reported to be useful for tracking the arrhythmia dynamics.[2;3] In the clinical setting such characterization is more restricted but new electrogram-based measures of activation fractionation and rate have been recently proposed for localization of ablation targets to improve efficacy in terminating AF.[4;5] Several studies describe

Correspondence: Omer Berenfeld, PhD, Center for Arrhythmia Research, University of Michigan, 5025 Venture Dr., Ann Arbor, MI 48109, oberen@umich.edu, Tel: 734-936-3500 Fax: 734-936-8266.

termination of AF in patients when ablation is performed at sites identified as exhibiting complex fractionated atrial electrograms (CFAEs).[6;7] In comparison, the study by Sanders et al. has shown that sites exhibiting the highest activation rate as measured by their dominant frequency (DF) are critical to the AF maintenance in patients.[5] To further rationalize the use of CFAE and DF for ablation guidance, Kalifa et al. demonstrated in isolated sheep hearts that these two measures may be predictably organized, whereby the most fractionated activity is found at the periphery of a source region having the highest activation rate.[8] In addition, experimental[9;10] and clinical[11] mapping studies have indicated that functional reentry underlies the highest activation rate and the maintenance of AF. However, the relationship between the spatiotemporal stability of such reentrant drivers and the fractionation and rate of the activation in their periphery has not been studied yet. Thus, the aim of this study was to investigate how the spatio-temporal characteristics of a cardiac fibrillation source that determine the DF of a local signal also contribute to the fractionation of that signal. Using the well established singular value decomposition (SVD) method[12] we analyzed numerical simulations and optical mapping data to test the hypothesis that the meandering pattern of a reentrant source that results in spatio-temporal instability and wave fractionation, is reflected in the power spectrum of local activity elsewhere in its surroundings and therefore may be used to trace the core of the source.

Methods

Detailed description of the methods can be found in the Online Supplement.

Numerical Data

Isotropic two-dimensional (2D) human atrial tissue was modeled using regular grids with 50-μm resolution. Reentrant sources were initiated by cross field stimulation (100ms coupling interval) and sustained fibrillatory activity was simulated in a uniform and a non-uniform model. For the non-uniform model, an effective interface for intermittent blockades was established by setting an ACh concentration ratio of 2:1 for the driver and standby areas, respectively. Transmembrane potential and pseudo electrograms were used for analysis.

Experimental Data

Experimental data were obtained from optical and electrical recordings in isolated Langendorff-perfused sheep hearts (n=5) during acute AF in the presence of acetylcholine (ACh, 1μM) and isoproterenol (3.2×10^{-8}M).

Spectral Analysis and DF

Power spectra were estimated from the fast Fourier transforms of zero padded to 2.048–4.096sec long signals (a resolution of 0.48–0.24Hz, respectively). The DF was defined as the frequency corresponding to the largest peak in the range 1–30Hz with enhanced resolution.[9]

Singular Value Decomposition and Periodicity

Time series (S) of either numerical transmembrane voltages, optical signals or electrograms, were decomposed into a periodic constituent (PC) related to an enhanced resolution DF, and a residual constituent (RC) related to all other activity by utilizing the singular value decomposition (SVD) method.[12]

To quantify the degree of periodicity in S we defined a new Periodicity Index (*PI*) based on the power levels of its PC and RC components in the time-domain, measured by the

standard deviation of these components around their mean values. The PI was calculated as follows:

$$PI_{SVD} = \frac{StD(PC)}{StD(PC)+StD(RC)}. \quad (1)$$

Thus, for a purely periodic signal *StD* (*RC*) = 0 and *PI*=1. The decomposition steps and validation are summarized in the Online Supplement (figures OS1–OS2).

To further link the non-periodic components of the activity, that are now standing-out clearly in the RC, to the source instability, we have introduced the *RC Tip Ratio*. Accordingly, the power spectrum of the RC was analyzed and the ratio of the spectral energy at the spiral tip circumnavigating frequency (F_{Tip}) and its modulatory peaks (F_{Mod}) to the total RC energy was calculated (see inset in figure 3).

RESULTS

Spectral Analysis of Rotor Meandering

First we demonstrate how the spectral properties of the tip trajectory of a reentrant source are reflecting the frequency of the rotation and its meandering pattern. Figure 1A presents an electrical activity snapshot in a uniform (left) and non-uniform (right) 5×5-cm models. The colors indicate voltage magnitude from rest (blue) to full depolarization (red). As indicated by the time-space plots, both models sustained rotational activity in their identical upper half with a frequency of ~22Hz. However, in the non-uniform case the rotational wave activity became fragmented and irregular in the lower half. To the right of the snapshots, time-space trajectories (TST) of the wavefront tip are given, in which the colors indicate the traveling time. The two tip trajectories outline a similar periodic octagon-star-like pattern. The completion time for the rotor-tip full cycle along the octagon was ~230ms (i.e. 4.3Hz). In addition we note that the time for the tip to travel along three edges (i.e. across three vertices, thus returning to a close vicinity of its starting location) was ~78ms (12.7Hz). In Figure 1B, the orthogonal projection of the tips' meandering trajectory on the *x*- and *y*-coordinates are plotted against time with their corresponding power spectra on their right. The spectra show a small peak reflecting the rotation frequency (F_{Rotor}=21.5Hz); however, it is notable that for both cases the highest peak corresponds to the tip meandering frequency (F_{Tip}=12.7Hz), rather than to the rate of electrical activation, which is the frequency of rotation.

Local Electrical Activity and the Singular Value Decomposition

Here we demonstrate how the spectral properties of the meandering reentrant source are reflected in the local activity of its surroundings. In figure 2, the SVD technique was applied to 4 locations of the model (a through d, as marked in figure 1A). The transmembrane signals, V_m, as well as their periodic and residual constituents are shown in panel A for points (a) and (b), and in panel B for points (c) and (d). The DF in the peripheral area of the non-uniform model was lower than in the source area (13 vs. 22Hz) and therefore point (d) was decomposed according to its local DF of 13Hz, resulting in a visibly slower periodic constituent time series (PC). The corresponding power spectra of the RCs are displayed to the right of the RC signals. As a reference, the pseudo unipolar electrograms at these points are shown on the right-most column. The RC power spectra at the 4 locations share three frequency peaks: the F_{Rotor} (21.9Hz), the F_{Tip} (12.9Hz) and a modulation frequency that equals the difference between the two (F_{Mod}, 9=21.9–12.9Hz). At location (d), which corresponds to the fibrillatory conduction area in the non-uniform model, additional multiple

spectral peaks appear, but still, in conjunction with F_{Rotor}, F_{Tip} and F_{Mod}. Thus, the rotor meandering characteristics shown in figure 1B are revealed in the form of additional RC peaks, leaving a signature in the non-periodic component of the activity in all 4 points. Moreover, comparison of the magnitude of the RC power at the 4 locations indicates that while in the uniform model the RC power decreases with distance from the rotor core (note different vertical scales in the RC spectrum at a and b), in the non-uniform model, it increases beyond the functional boundary. A generalization of these analyses along the profiles marked in figure 1A is demonstrated in the online supplemental results (figure OS3).

Quantifying Irregularity in the Core Periphery

In figure 3A, spatial maps of periodicity index, PI, for the 2 model types are shown on the left column. In the uniform model, the map shows a high level of periodicity all over the 2D domain, with the exception of a narrow disk area of decreased periodicity at the spiral tip meandering region (i.e. the region covered by the octagon trajectory patterns shown in figure 1). In the non-uniform tissue, a sharp drop in periodicity occurs along the boundary between the two functional regions, and periodicity gradually increases underneath the interface.

It has been already demonstrated in figures 2 and OS3 that the residual constituents obtain frequency components from both the meandering and the spiral wave rotation. To quantify the contribution of the tip meandering to irregularity we calculated the RC tip ratio as presented in the Methods. To the right of the PI maps in figure 3A, RC tip ratio maps are given for the 2 model types. A comparison of the PI and the RC tip ratio maps and traces as presented in figures 3B and 3C reveals an opposite relationship in their large peaks and troughs, with asymmetric recovery distal to the intermittent blockade line. Nevertheless the profile plots in figures 3B and 3C, corresponding to the dashed white lines in panel A, highlight some differences: first, in the vicinity of the tip meandering region, the RC tip ratio is more sensitive to the distance from the meandering center than the PI. The PI values in figure 3B drop around the meandering center with a symmetric Gaussian-like shape with a narrow width (3mm at half height), whereas the RC tip ratio values in figure 3C obtain a much broader pattern (11mm at half height). Second, the PI does not reliably distinguish between reduced regularity due to meandering region or intermittent blockades, as they both leave almost similar signatures along the profile. Conversely, the RC tip ratio in figure 3C shows distinct morphology signatures at the regions of meandering and intermittent blockade. While the RC tip ratio decreases symmetrically on both sides of the rotor core, it decreases only to about half of its peak value toward the side corresponding to the low [ACh] (i.e. the bystander half sustaining fibrillatory conduction). This partial decrease is understood by noting that the RC spectral peaks in the fibrillatory region maintain their power at increasing distances from the boundary with the 1:1 propagation region (see figure OS3).

Meandering Magnitude Controls Residual Constituents

To gain mechanistic insight into the origin of the irregularity in the core periphery we analyzed how the meandering pattern of the tip affected local propagation directionality as well as local activation. Our results presented in the Online Supplement (figure OS4) demonstrate that the waves that emanate from the meandering source undergo a consistently periodic shift in their directionality concomitant with periodic modulation in local activation cycle length, all sharing the same spectral components, thus directly relating meandering to the residual constituents and irregularity of the local electrical activity in the core periphery.

Figure 4 shows the effects of increasing the magnitude of tip meandering on the spectral density. The meandering amplification was obtained by increasing the diffusion coefficient

from a reference value of 0.1 mm^2/ms (×1) to 0.3 and 0.6 mm^2/ms (×3 and ×6, respectively). Similar ionic kinetics were used in all cases on a uniform 1×1-cm sheet giving rise to rotation with a relatively similar frequency. Nevertheless, the top of figure 4A shows that the increase in diffusion coefficient increased the excitation wavelength and the meandering excursion of the tip trajectory (1.6, 2.0, and 2.7 mm for ×1, ×3 and ×6, respectively). For the x1 case, the tip meandering profile illustrated by the TST at the middle row of figure 4A demonstrated two periodicities – the tip traveled around a square-like trajectory with a cycle length of $T_{1\rightarrow2}\approx$130ms (7.8Hz, where $T_{1\rightarrow2}$ is the travelling time between points 1 and 2); and the deformed square itself slowly rotated anti-clockwise, completing a full rotation in $T_{1\rightarrow1}\approx$422ms (2.37Hz; i.e. the tip returned to its original location with a $T_{1\rightarrow1}$ periodicity). Representative pseudo unipolar electrograms for the three models at the same location (asterisks) are shown in the lower row in panel A, demonstrating increased fractionation with increased meandering excursion.

The predominance of the partial meandering cycle $T_{1\rightarrow2}$ in the spectral content of the tip trajectory is illustrated in the top traces of the figure 4B, where the spectra of the tip *x*-coordinate are shown. In the bottom traces of figure 4B, the RC spectrum of the x1 case shows that decomposition into periodic and residual constituents of a signal recorded distal to the core (asterisks in panel A), revealed the tip meandering properties. The RC resulted in a significant frequency component at 7.5Hz (F_{Tip}), corresponding to $T_{1\rightarrow2}$ within our frequency resolution. The peak at 25.5Hz reflected the temporal properties of the spiral rotation (F_{Rotor}). An additional frequency peak was noticed at 18Hz that represented the modulation of the rotation frequency by the tip's trajectory along four edges of the deformed square (18=25.5–7.5Hz). For the x3 and x6 models, while the duration of the tip traveling along four edges of the square was similar (97 and 95ms for the ×3 and ×6, respectively), the time needed for the tip to return to its starting point was longer in the latter ($T_{1\rightarrow1}$ =260 and 450ms, or 3.85 and 2.22Hz, for the ×3 and ×6, respectively). Overall, the 3 spectra at the bottom of panel B clearly show that relative to the spiral power at F_{Rotor}, the power associated with the tip meandering (at F_{Tip} and F_{Mod}) increases with the meandering excursion area. Comparable to the reference x1 case, the RC showed similar frequency components as in the spectra of the rotor tip coordinate (i.e. $1/T_{1\rightarrow2}$).

We have applied the SVD technique on pseudo unipolar electrograms all over the 2D domain for the three simulations of figure 4. The results are given in the Online Supplement (figure OS5) and show that also in electrograms, the reduced periodicity index near a meandering rotor results, at least in part, from tip meandering. This reduction is related to spectral peaks in the RC at frequencies that reflect tip meandering, its harmonics and its modulation by the faster rotor frequency. The relative contribution of the meandering components to the RC spectrum is indicative of the distance from the measuring point to the center of meandering. The spatial extent of reduced periodicity is increased with increased diameter of spiral core meandering.

Rotor Meandering and Local Fractionation in Experiments

We tested the numerical predictions using movies of the electrical activity from the left atrial (LA) free wall or the posterior left atrium (PLA) of isolated sheep hearts. An experimental example for the effect of meandering on irregularity of activity is given in figure 5. In panel A, a phase map at the LA free wall (left) shows a snapshot of a clockwise rotor found to rotate at ~7.8Hz and to drive the overall atrial activity (blue, full repolarization; yellow, full depolarization). Tracking the rotor tip's TST (middle) and calculating the spectra of the *x*- and *y*-coordinates (right) showed a significant frequency component at 3.9Hz, and additional, less prominent components at ~2.3 and 7.8Hz. Decomposition of the optical signals into the periodic and residual constituents demonstrated again the association of the tip meandering spectral properties to the RC. A

representative example is given in figure 5B for the point marked on the phase map with an asterisk. The upper trace shows the optical signal, while the lower traces are the original (S) and decomposed constituents (PC and RC) power spectra. Not only was the tip meandering component reflected as a dominant peak of 4.0Hz in the RC spectra on the LA, where the driving rotor existed, but also on the right atrium, where activation was much less regular (data not shown). We have also determined the PI and the RC tip ratio as a function of distance from the center of tip meandering along the dashed line on the map in panel A. As shown in figure 5C, the numerical predictions are clearly borne out by both curve morphologies (compare to figure OS5 B–C). The PI sharply increased from the core region from a value of ~0.25 to a stable value of ~0.75 at a distance of ~3 mm from the core, thus being insensitive to the distance from the center of activity at the periphery. On the contrary, the RC tip ratio decayed exponentially from the meandering perimeter, with a characteristic distance of λ=1.3mm and a 0.2 value at ~8mm away from the center. Such a behavior shows that the effect of meandering extends beyond its trajectory area and suggests that relative magnitudes of the tip components in the RC spectrum may be used to indicate the distance to the rotor core. The exponential patterns of the PI and the RC tip ratio from the meandering border towards the periphery were verified in 4 additional optical mapping experiments with recordings from either the free or the posterior LA walls and similar analysis. The summary table 1 shows the high correlation of the exponential decay best-fitting to the RC tip ratio data (R=0.95±0.04), and that the characteristic spread distance was λ=1.43±0.21mm, supporting the applicability of our observations to atrial fibrillation episodes sustained by a quasi-stable rotor. Similarly, in 4 of the 5 experiments we obtained a good PI fit with an exponential form as in figure 5C (R=0.97±0.01, table 2).

DISCUSSION

This study aimed at better understanding the basis of fractionated cardiac electrical signals using a new approach based on singular value decompositions (SVD) in the time-domain, which allows extraction of two underlying contributions - periodic and residual constituents. We propose here that, at least in scenarios of quasi-stable rotor activity, an analysis of such constituents can be used for quantification of periodicity of activation during AF. Importantly, the residual constituent can be used to characterize specifically the role of a reentrant source in irregular and fractionated activity.

Meandering as a Source of Irregularity

We demonstrated that the frequencies associated with meandering of a quasi-stable rotor are reflected in the power spectra of measured signals outside its immediate vicinity, and thus provide a mechanism for local irregularity and electrogram fractionation. We showed also that the meandering frequency properties determine beat-to-beat changes in local directionality and cycle length between successive activations, and thus are a direct mechanism of fractionation. The directionality oscillations are readily attributable to the spatial shift of the origin of the wave (figure OS4A). However, the oscillations in the local cycle length outside the core region may be attributable to a combination of complex restitution of refractory period as well as the Doppler effect on the local activation rate. According to the latter, the shift of the origin of the waves towards and away from the recording point accelerates and slows the activation rates, respectively.[13] The data on transmembrane voltage presented in figure OS4 also confirm that fractionation may be a result of variability in local activity, and not only the result of core activity detection by far-field probing with the unipolar electrode, as might be suspected for the fractionated signals presented in figure 4.

Generally, the frequency components of the RC overlapped with those of the PC. For example, the rotation frequency in the uniform and non-uniform models presented in figures

1 to 3 was about 22Hz, which was the fifth harmonic of the frequency related to a complete cycle of the tip along the octagon-star trajectory (230ms or 4.4Hz, see figure 1A), so that 4.4×5=22Hz. Similarly, in the set of simulations presented in figure 4, the spiral wave rotation frequency was a high harmonic of the full-cycle rotation frequency of the spiral tip ($1/T_{1\rightarrow1}$, 11^{th}, 7^{th} and 12^{th} harmonic for the x1, x3 and x6 cases, respectively). Also in the experimental example shown in figure 5, it is clear that the rotor reverberating frequency of 7.8Hz is the second harmonic of the tip meandering frequency of 3.9Hz. Overall, in all 5 experiments the rotor frequency was found to be the second or third harmonic of the tip meandering frequency (see Table 1). Our interpretation is that the DF and its harmonics can themselves be harmonics of a slower frequency that corresponds to the meandering pattern, implying coupled rather than independent activities, one resonating the other. Consequently, frequency-based separation of the two activities into two distinct, mutually exclusive, frequency bands may be limited.

In both optical and unipolar electrograms, the balance between the spectral components of the RC peaks that relate to the tip meandering and the total RC power (RC tip ratio) was found to depend on the distance between the measurement point and the core, as well as the core size. Moreover, meandering may leave a unique Gaussian-like signature on the RC tip ratio profile as compared to that of intermittent blockades (unlike PI) thus, suggesting the possibility of differentiating between these two sources of fractionation.

The SVD and Irregular Activity

Arguably, the characterization of the spatiotemporal properties of an AF source is critical if one wishes to advance AF therapeutic procedures, specifically via ablation. Recently, the usefulness of DF and CFAE spatial maps was investigated for its potential contribution to atrial ablation success rates.[14] The study showed that it is feasible to use electrogram guided ablation, where the reentrant source is tracked due to its high correlation with the maximal DF and fractionated electrograms. However, the results were inconsistent.[14]

Regularity indices are intended to quantify the periodicity or organization of the measured signal, be it an electrogram or membrane voltage signal measured by optical mapping. Several approaches for determination of regularity have been used, both in time-domain (CFAEs)[6] and in frequency-domain (RI[8] and OI[3]). Both approaches pose some limitations: The first approach is limited by its categorical definition and the latter two approaches by relying on the assumption that activity at DF can be isolated from other activity in the frequency domain, which may be inaccurate. The SVD-based periodicity, or regularity, measure proposed here is devoid of such limitations.

SVD Clinical Applicability

The SVD presents an intuitive way to attribute the spectral characteristics of the residual signal to that of the rotor tip and may help to remotely characterize source stability during mapping of AF in humans. Within the frame of our study limitations (see Online Supplement for further details), this approach may be particularly useful when only relatively low resolution mapping is available. As part of our technique validation, experimental examples demonstrated high correlation between the periodicity indices that are measured from the optical signals and the unipolar electrograms, demonstrating the potential applicability of the proposed methodology for atrial mapping during ablation procedures (figures OS6–7). In addition, SVD-based regularity assessment of CFAEs recorded from patients[6] demonstrated feasibility of quantifying the otherwise empirical definition of complex fractionated electrograms (figure OS8). Another possible advantage of the SVD method presented here is that, based on simulation data presented in figure 3, spatial information on PI and RC tip ratio may be used to distinguish fractionation

associated with fibrillatory activity from one associated with a rotor driving AF, and as such potentially reduce the extent of ineffective ablation. Lastly, accounting for 70 randomly selected signals in our experiments, the median ratio between the power at the meandering peaks (F_{Tip} and F_{Mod}) and the maximal value of the RCs' power was 24.9%. That ratio, being clearly higher than a typical noise level of 5%, suggests that the tip meandering related frequencies could be detected in the clinical practice.

Supplementary Material

Refer to Web version on PubMed Central for supplementary material.

Acknowledgments

Supported in part by NHLBI Grants PO1-HL039707, P01-HL087226, RO1-HL070074-05A1, RO1-087055-01, AHA SDG 0230311N, and ACCF/GE Healthcare Career Development Award.

Reference List

1. Jalife J, Berenfeld O, Skanes A, et al. Mechanisms of atrial fibrillation: mother rotors or multiple daughter wavelets, or both? J Cardiovasc Electrophysiol. 1998; 9:S2–12. [PubMed: 9727669]
2. Akar JG, Everett TH, Kok LC, et al. Effect of electrical and structural remodeling on spatiotemporal organization in acute and persistent atrial fibrillation. J Cardiovasc Electrophysiol. 2002; 13:1027–1034. [PubMed: 12435191]
3. Everett TH, Wilson EE, Verheule S, et al. Structural atrial remodeling alters the substrate and spatiotemporal organization of atrial fibrillation: a comparison in canine models of structural and electrical atrial remodeling. Am J Physiol Heart Circ Physiol. 2006; 291:H2911–H2923. [PubMed: 16877548]
4. Ryu K, Sahadevan J, Khrestian CM, et al. Use of fast fourier transform analysis of atrial electrograms for rapid characterization of atrial activation-implications for delineating possible mechanisms of atrial tachyarrhythmias. J Cardiovasc Electrophysiol. 2006; 17:198–206. [PubMed: 16533258]
5. Sanders P, Berenfeld O, Hocini M, et al. Spectral analysis identifies sites of high-frequency activity maintaining atrial fibrillation in humans. Circulation. 2005; 112:789–797. [PubMed: 16061740]
6. Nademanee K, McKenzie J, Kosar E, et al. A new approach for catheter ablation of atrial fibrillation: mapping of the electrophysiologic substrate. J Am Coll Cardiol. 2004; 43:2044–2053. [PubMed: 15172410]
7. Rostock T, Rotter M, Sanders P, et al. High-density activation mapping of fractionated electrograms in the atria of patients with paroxysmal atrial fibrillation. Heart Rhythm. 2006; 3:27–34. [PubMed: 16399048]
8. Kalifa J, Tanaka K, Zaitsev AV, et al. Mechanisms of wave fractionation at boundaries of high-frequency excitation in the posterior left atrium of the isolated sheep heart during atrial fibrillation. Circulation. 2006; 113:626–633. [PubMed: 16461834]
9. Mandapati R, Skanes A, Chen J, et al. Stable microreentrant sources as a mechanism of atrial fibrillation in the isolated sheep heart. Circulation. 2000; 101:194–199. [PubMed: 10637208]
10. Sarmast F, Kolli A, Zaitsev A, et al. Cholinergic atrial fibrillation: I(K, ACh) gradients determine unequal left/right atrial frequencies and rotor dynamics. Cardiovasc Res. 2003; 59:863–873. [PubMed: 14553826]
11. Atienza F, Almendral J, Moreno J, et al. Activation of inward rectifier potassium channels accelerates atrial fibrillation in humans: evidence for a reentrant mechanism. Circulation. 2006; 114:2434–2442. [PubMed: 17101853]
12. Kanjilal PP, Palit S, Saha G. Fetal ECG extraction from single-channel maternal ECG using singular value decomposition. IEEE Trans Biomed Eng. 1997; 44:51–59. [PubMed: 9214783]
13. Gray RA, Jalife J, Panfilov AV, et al. Mechanisms of cardiac fibrillation. Science. 1995; 270:1222–1223. [PubMed: 7502055]

14. Lemola K, Ting M, Gupta P, et al. Effects of two different catheter ablation techniques on spectral characteristics of atrial fibrillation. J Am Coll Cardiol. 2006; 48:340–348. [PubMed: 16843185]

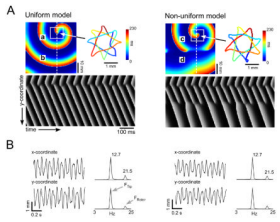

Figure 1.

Tip meandering and the power spectrum. A) Snapshots of spiral wave activity with octagon star-like meandering tip in uniform (left) and non-uniform (right) models. The tip was identified in the corresponding phase map as the point at which all phases converged. The tip trajectory was assembled by joining the tip locations in each consecutive frame; a-d sites of recordings in figs 2 and 3. Time-space plots of activity along the dashed white lines are shown at bottom; B) Tip x-y-coordinate signals and corresponding power spectra, for uniform (left) and nonuniform (right) models, both showing a dominant peak at 12.7 Hz.

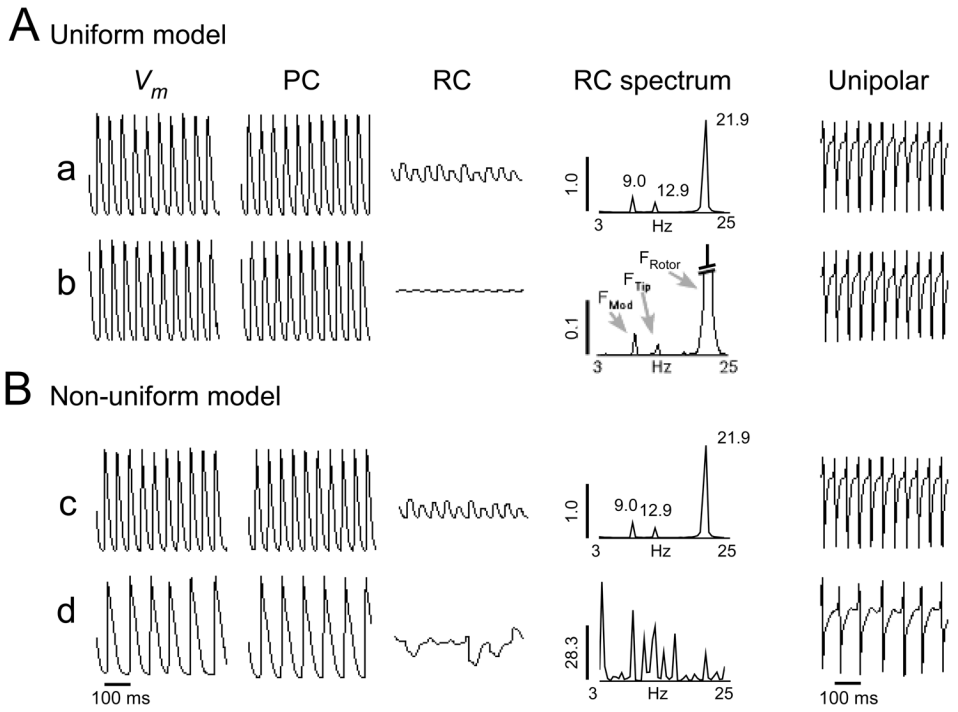

Figure 2.

A) Signal decomposition into periodic and residual constituents (RCs) at locations a and b as marked in figure 1A. All signals are shown with the same ordinate scale. The power spectra of the RCs are shown to their right, the pseudo unipolar electrograms are shown on the right-most column. B) Results for points c and d displayed as in panel A.

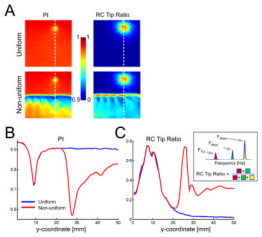

Figure 3.

Quantifying irregularity in the core and its periphery. A. Two-dimensional maps of periodicity index (PI) and residual component (RC) tip ratio. B and C vertical profiles of PI and RC tip ratio, respectively, along the line marked in panel A. The inset provides a diagrammatic definition of RC tip ratio in a simplified power spectrum with a total of 3 peaks, two of which correspond to the spiral tip meandering.

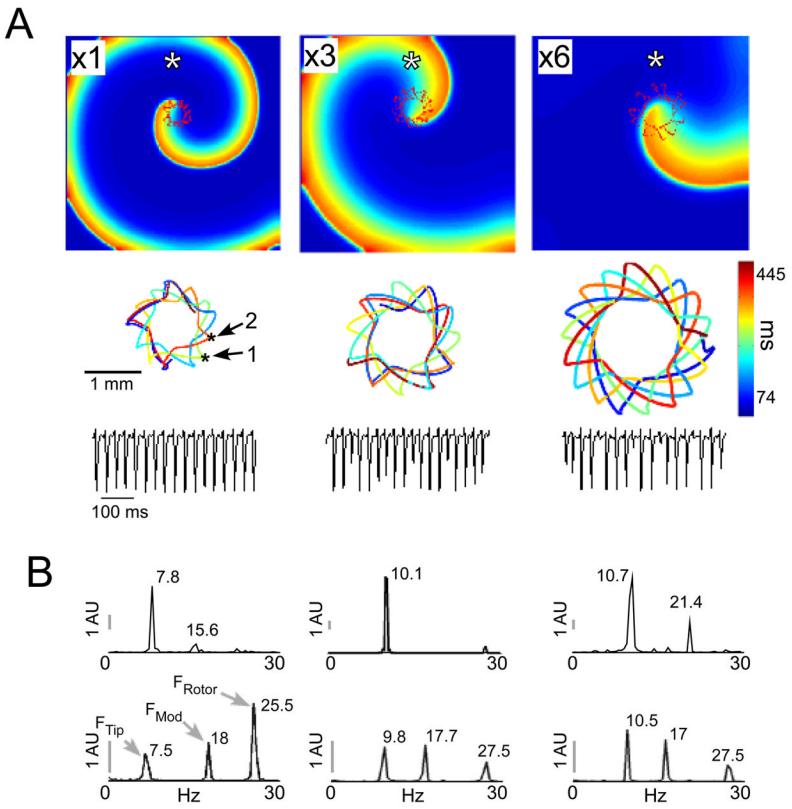

Figure 4.

Meandering magnitude and fractionation, A) Spatiotemporal characteristics of the spiral wave tip in uniform model. Diffusion coefficient ratio is 1:3:6 for left, middle and right columns, respectively. Top, snapshots of spiral wave activity with tip trajectory in red. Middle, spatiotemporal trajectories of meandering tip (kink in the initial x6 tip trajectory corresponds to a transient stabilization phase). Bottom, pseudo unipolar electrograms at a single location (white asterisks spiral snapshots) show increased irregularity with increasing meandering diameters. B) Top - power spectra of the spiral tip *x*-coordinate. Bottom - Power spectra of the residual constituent (RC) of the signals measured. Scale bars – 1 power spectral arbitrary unit.

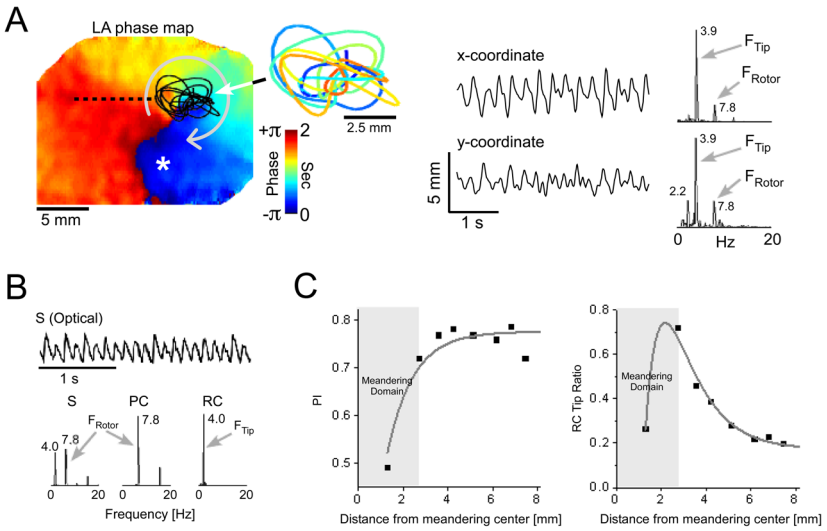

Figure 5.

Rotor meandering and fractionation in optical mapping experiment during AF in isolated sheep heart. A) Left atrial phase snapshot demonstrating reentrant activity in the LA free wall. The time-space trajectory of the tip, the *x* and *y*-coordinate signals and their corresponding spectra are shown on the right. B) Power spectra of a single optical signal (S) and its periodic and residual constituents (PC and RC) at the location marked by an asterisk in panel A. The original optical signal is shown at the top trace. C) PI and RC tip ratio as a function of the distance from the meandering center along black dashed line in A.